

# Reconstructing Hyperons with the $\overline{\text{PANDA}}$ Detector at FAIR

**W Ikegami Andersson**

**on behalf of the  $\overline{\text{PANDA}}$  collaboration**

Department of Physics and Astronomy, Uppsala University, Box 516, S-751 20 Uppsala, Sweden

E-mail: [walter.ikegami\\_andersson@physics.uu.se](mailto:walter.ikegami_andersson@physics.uu.se)

**Abstract.** Hyperon production and the study of their properties is an important part of the physics programme of the future  $\overline{\text{PANDA}}$  experiment at FAIR. Antihyperon-hyperon pairs will be produced in antiproton-proton collisions through the annihilation of at least one light antiquark-quark ( $u, d$ ) pair and the creation of a corresponding number of antiquark-quark  $\bar{s}s$  pairs. By measuring the decay products of the hyperons, spin observables such as the polarisation can be measured.

Many hyperons have a long life-time which gives rise to final state particles originating from displaced vertices. A pattern recognition algorithm using information from the  $\overline{\text{PANDA}}$  Straw Tube Tracker is extended to reconstruct not only the transversal, but also the longitudinal components of charged tracks. A Hough transform and a path finding method as tools to extract the longitudinal components are being developed.

## 1. Introduction

Quantum chromodynamics (QCD) is the theory of strong interaction, one of the four fundamental forces, and a part of the Standard Model. QCD describes the interaction between quarks and gluons which constitute the visible matter in the universe. In contrast to the electromagnetic and the weak interactions, the coupling constant  $\alpha_s$  of the strong interaction diminishes over short distances and increases over long distances. At short distances, or high energy interactions, perturbation theory can be applied to perform QCD calculations. In low energy interactions,  $\alpha_s$  grows large and perturbation theory can no longer be used. Instead, numerical methods or effective field theories, such as chiral perturbation theory, where hadrons act as degrees of freedom, can be used. The relevant degrees of freedom for an interaction are given by the energy scale. The energy scale where perturbative QCD is no longer applicable is called the QCD cut-off and is  $\Lambda_{QCD} \approx 200$  MeV [1]. The energy scale of hyperon production in  $\bar{p}p \rightarrow \bar{Y}Y$  reactions is given by the strange quark mass  $m_s \approx 100$  MeV, which is close to the QCD cut-off. As a consequence, the relevant degrees of freedom are unclear and predictions hard to make. Instead, phenomenological models have to be developed. Various  $\bar{p}p \rightarrow \bar{Y}Y$  reactions have been described in both a quark-gluon picture [2], in a hadron picture [3] as well as the combination of the two [4]. These models give different predictions for *e.g.* the polarisation. Therefore, measuring the spin observables of  $\bar{p}p \rightarrow \bar{Y}Y$  reactions will help to further develop the models in the intermediate energy domain.



The foreseen  $\overline{\text{PANDA}}$  (antiProton ANnihilation at DArmstadt) detector at FAIR (Facility for Antiproton and Ion Research) provides unique opportunities for hyperon production. The experiment will provide the near  $4\pi$  coverage needed to completely measure the angular distribution of the final state particles and subsequently measure spin observables. Since ground state hyperons decay weakly, they have a significantly long life-time and can travel a macroscopic distance from the interaction point.

In the following sections, spin observables in the  $\overline{p}p \rightarrow \overline{Y}Y$  reaction, where  $Y$  refers to a hyperon, are discussed. The development of pattern recognition algorithms dedicated for charged particles originating from displaced vertices is also presented.

## 2. Spin observables in $\overline{p}p \rightarrow \overline{\Lambda}\Lambda$ reactions

The spin variables for the  $\overline{p}p \rightarrow \overline{Y}Y$  reaction are derived using the density matrix formalism [5]. The density matrix for a single particle with spin  $j$  is given by

$$\rho = \frac{1}{2j+1} \mathcal{I} + \sum_{L=1}^{2j} \frac{2j}{2j+1} \sum_{M=-L}^L Q_M^L r_M^L, \quad (1)$$

where  $\mathcal{I}$  is the identity matrix,  $Q_M^L$  are Hermitian matrices,  $r_M^L$  are the polarisation parameters,  $L$  is the angular momentum and  $M$  its third component [6]. For spin- $\frac{1}{2}$  particles,  $Q_M^L$  are the Pauli matrices and  $r_M^L$  can be interpreted as the vector polarisations  $P_x, P_y$  and  $P_z$ , and the density matrix becomes

$$\rho(1/2) = \frac{1}{2} \begin{bmatrix} 1 + P_z & P_x + iP_y \\ P_x - iP_y & 1 - P_z \end{bmatrix}. \quad (2)$$

Since the  $\overline{p}p \rightarrow \overline{Y}Y$  reaction is a strong process, parity must be conserved. This imposes constraints on the polarisation:  $P_x = P_z = 0$ . The density matrix of the final state then reduces to

$$\rho(1/2) = \frac{1}{2} \begin{bmatrix} 1 & iP_y \\ -iP_y & 1 \end{bmatrix}. \quad (3)$$

Because of the parity violating weak decay of hyperons, the spin observables of the  $\overline{p}p \rightarrow \overline{\Lambda}\Lambda$  reaction can be accessed by the angular distribution of the decay particles. One example is the weak  $\Lambda \rightarrow p\pi^-$  decay that has a branching ratio of  $\text{BR}(\Lambda \rightarrow p\pi^-) = 63.9\%$  [7]. The angular distribution of the final state particles is [6]

$$I(\theta_p) = \frac{1}{4\pi} (1 + \alpha_\Lambda P_y \cos \theta_p), \quad (4)$$

where  $\alpha_\Lambda = 0.64$  [7] is the decay parameter and  $\theta_p$  is the polar angle of the proton. The polar angle  $\theta_p$  is measured in the  $\Lambda$  rest frame between the direction of the outgoing proton and the axis normal to the production plane (see Figure 1a). Thus, by measuring the scattering angle of the proton, the polarisation  $P_y$  can be deduced. In an experiment with unpolarised beam and unpolarised target such as  $\overline{\text{PANDA}}$ , the polarisation of the individual hyperons as well as the spin correlation between the two are accessible.

The density matrix formalism has also been used to derive angular distributions of the  $\Xi^- \rightarrow \pi^- \Lambda \rightarrow \pi^- \pi^- p$  and  $\Omega^- \rightarrow K^- \Lambda \rightarrow K^- \pi^- p$  hyperon decay chains. Since the  $\Omega^-$  hyperon has spin- $\frac{3}{2}$ , the situation is more complicated. Instead of one non-zero polarisation parameter as in the spin- $\frac{1}{2}$  case ( $P_y$ ) there are seven. These have been derived in [6].

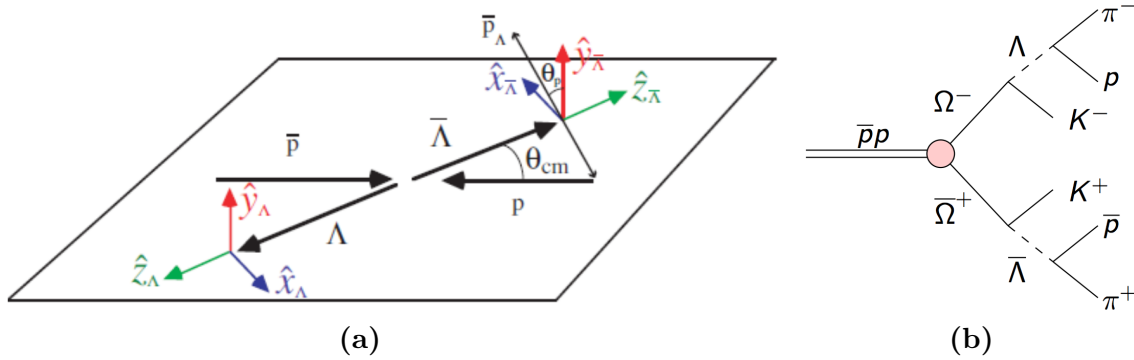


**Figure 1.** (a) Production plane of the  $\bar{p}p \rightarrow \bar{\Lambda}\Lambda$  reaction. The  $y$ -axis of the  $\Lambda$  rest frame is perpendicular to the production plane. (b) The  $\Omega^+\Omega^- \rightarrow K^+\pi^+\bar{p}K^-\pi^-p$  reaction channel.

### 3. Pattern recognition with the $\bar{P}$ ANDA Straw Tube Tracker

Simulations and measurements have shown that hyperons can travel tens of centimeters from their production vertex before decaying due to their long life-times. Furthermore, channels such as  $\Omega^- \rightarrow K^-\Lambda \rightarrow K^-\pi^-p$  (see Figure 1b) produce additional displaced vertices from the production of a  $\Lambda$  in the first decay. This makes it challenging to reconstruct hyperon events as the information about the decay points is *a priori* unknown.

The  $\bar{P}$ ANDA detector will have several subdetectors for detecting charged particles. These include a Micro Vertex Detector (MVD), a Straw Tube Tracker (STT) and Gas Electron Multiplier (GEM) disks as well as a Forward Tracking System (FTS). Charged tracks originating from a hyperon decay could leave only a few hits or completely miss the MVD and/or the GEM disks, leaving only information in the STT. Here, particular attention is given to the STT.

The STT consists of 4636 gas filled straws. There are inner and outer segments which contain layers of straws parallel to the beam direction. In between, there is a skewed segment, where straws have been tilted by  $\pm 2.9^\circ$ . The straws have a conductive inner layer and an anode wire in the center. A potential difference is applied between the conductor and the wire. When an ionizing particle traverses a straw, gas atoms in the particle trajectory are ionized, creating free electrons and ions. The electric field causes electrons to travel to the wire, producing an electric signal. A relation between the drift time and the radial distance to the wire of an electron is obtained through a calibration procedure. This relation is used to calculate the closest radial distance of a trajectory to the wire. The radius is called the isochrone and can be imagined as a cylinder along the wire representing all possible track positions [8].

In the  $\bar{P}$ ANDA software, a standard track finding algorithm exists for the detection of charged particles originating from the interaction point. In the case of hyperon decays, some tracks can only be reconstructed within the STT due to the displaced vertices. The standard track finder is not suited for the detection of such events and a different algorithm is required. A pattern recognition algorithm that can operate with only information from the STT has been developed in [9]. In this algorithm, a particle trajectory is assumed to be a perfect helix *i.e.* no energy losses and a homogeneous magnetic field are considered. A clusterization is done where parallel straws giving a signal are grouped together if the straws are adjacent to each other. A clusterization procedure is also performed to group together the skewed straws. After the clusterization is complete, a circle is fitted tangential to the isochrones of all parallel straws. This circle represents the particle track in the  $xy$ -projection. In Figure 2a, a  $\bar{p}p \rightarrow \bar{\Lambda}\Lambda \rightarrow \bar{p}\pi^+p\pi^-$  event is shown, where four tracks are found. The projected isochrones (purple circles) are tangent to the tracks (black circles).

This algorithm is now being extended to reconstruct the longitudinal position  $z$  and

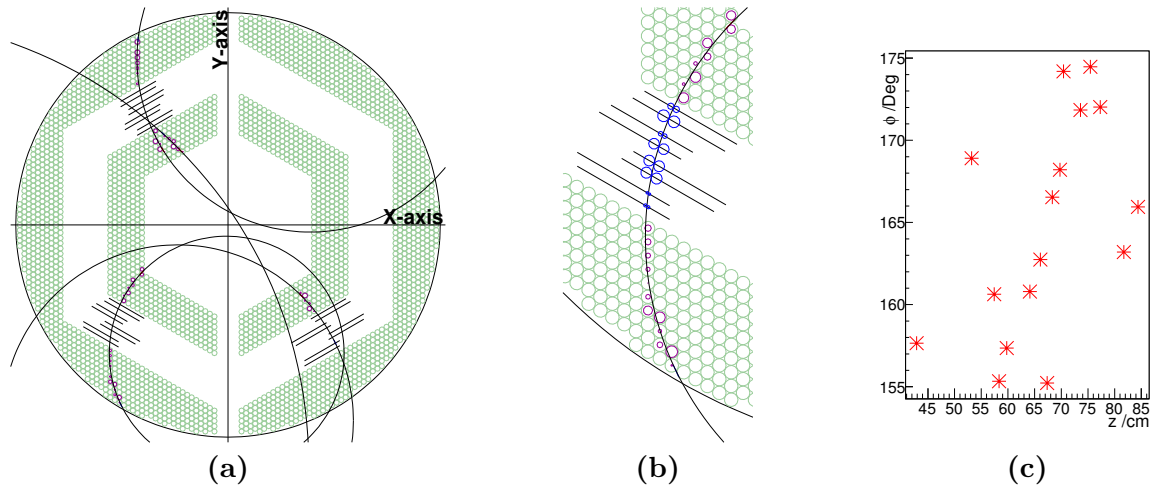


**Figure 2.** (a)  $xy$ -projection of the STT with a reconstructed  $\bar{p}p \rightarrow \bar{\Lambda}\Lambda \rightarrow \bar{p}\pi^+p\pi^-$  event at  $p_{beam} = 1.64$  GeV/c is shown. (b) Bottom-left track from Figure 2a. The possible isochrone positions are centered in the skewed straws and tangential to the track. (c) The resulting  $(z, \phi)$  coordinates of the isochrone centers from the track in Figure 2b.

momentum  $p_z$ , giving a full 3D view of a particle trajectory. The  $z$ -position where the particle traversed a skewed straw is determined by aligning the isochrone to the track. The  $xy$ -projection of the isochrone in a skewed straw is an ellipse. The ellipse is aligned such that it is tangential to the track and centered along the straw wire, shown in Figure 2b. For each skewed straw, there are two possible ways the isochrone can be aligned, analogous with a left-right ambiguity. Two possible solutions to this ambiguity are currently under development.

### 3.1. The Hough transform

One solution to the ambiguity problem is the *Hough transform*. It is a feature extraction method used to find geometric shapes in images [10]. The track helix is a straight line in  $(z, \phi)$  space. The correct points in the skewed straws are found by finding the line which crosses the most points with the Hough transform. Instead of the common Cartesian parametrisation of a line, the Hesse normal form is used. A line is represented by its closest distance  $r$  to the origin and the angle  $\theta$  [11]

$$r = x \cos \theta + y \sin \theta. \quad (5)$$

For each  $(z, \phi)$  point (see Figure 2c), a set of lines in steps of  $1^\circ$  are generated. In Figure 3a a set of lines at a point is shown. The line parameters are stored in a histogram called the accumulator space, shown in Figure 3b. After the accumulator space has been filled, a "voting procedure" begins where a maximum is searched for in the accumulator space. The parameters at the maximum correspond to the line that crosses the most  $(z, \phi)$  points, referred to as the *Hough line*. For each skewed straw, the distance of the two possible points to the Hough line is evaluated and the point furthest away is discarded. A straight line fit is performed with the remaining point in every skewed straw. The resulting slope parameter is used to calculate the helix angle and the longitudinal momentum and position are derived.

### 3.2. The Path finding method

A second method is being developed by taking a combinatorial approach. For each pair of neighbouring skewed straws, lines are calculated between all combinations of  $(z, \phi)$  coordinates,

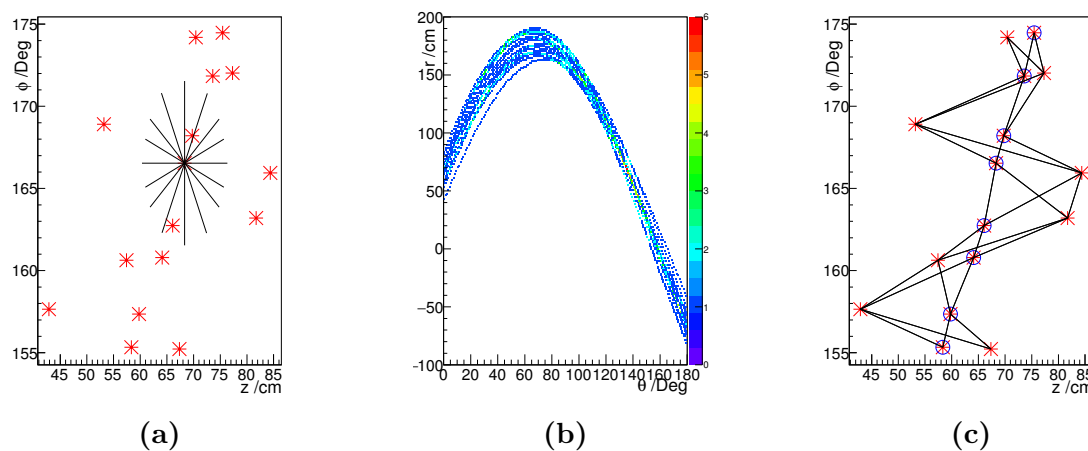


**Figure 3.** (a) A set of lines generated for one  $(z, \phi)$  point. Only a couple of lines are shown. (b) The accumulator space after all lines have been generated for all points. (c) All generated lines in the path finder approach. The encircled  $(z, \phi)$  points are chosen as correct points.

shown in Figure 3d. The angle is calculated between all pairs of lines that connect to each other at a  $(z, \phi)$  point. The correct set of points is found by looking for a path from the innermost to the outermost skewed straw along the lines and calculating a weight

$$w = \sum_i \pi - \theta_i, \quad (6)$$

where  $\theta_i$  is the angle between two lines at point  $(z_i, \phi_i)$ . To reduce the number of possible paths, a constraint requiring an angle to be above a certain value  $\theta_i > \theta_{cut}$  is introduced. A path containing an angle smaller than  $\theta_{cut}$  is removed. The  $(z, \phi)$  points along the path with the smallest weight  $w$  are chosen as the correct positions and a straight line fit is performed. As before, the helix angle is obtained and the longitudinal momentum and position are calculated.

## References

- [1] Ellis R K, Stirling W J and Webber B R, *QCD and Collider Physics* (Cambridge Monographs on Particle Physics, Nuclear Physics and Cosmology, vol. 8, Cambridge University Press, 1996)
- [2] Kohno M and Weise W, Phys. Lett. B **179**, 15 (1986); Rubinstein H R and Snellman H, Phys. Lett. B **165**, 187 (1985); Furui S and Faessler A, Nucl. Phys. A **468**, 669 (1987); Burkardt M and Dillig M, Phys. Rev. C **37**, 1362 (1988); Alberg M A et al., Z. Phys. A **331**, 207 (1988)
- [3] Tabakin F and Eisenstein R A, Phys. Rev. C **31**, 1857 (1985); Kohno M and Weise W, Phys. Lett. B **179**, 15 (1986); La France P et al., Phys. Lett. B **214**, 317 (1988); Timmermans R G E et al., Phys. Rev. D **45**, 2288 (1992); Haidenbauer J et al., Phys. Rev. C **46**, 2516 (1992)
- [4] Ortega P G et al., Phys. Lett. B **696**, 352 (2011)
- [5] J J Sakurai, *Modern quantum mechanics*, (Addison-Wesley, 1994)
- [6] Thomé E, *Multi-Strange and Charmed Antihyperon-Hyperon Physics for PANDA*, Acta Universitatis Uppsaliensis, Uppsala Dissertations from the Faculty of Science and Technology 101 (Ph. D. Thesis, Uppsala University, 2012)
- [7] K A Olive et al. [Particle Data Group Collaboration], Chin. Phys. C **38** (2014) 090001.
- [8] W. Erni et al. [PANDA Collaboration], Eur. Phys. J. A **49**, 25 (2013) [arXiv:1205.5441 [physics.ins-det]].
- [9] Schumann J, *Beschleunigung eines Spurfindealgorithmus für den Straw Tube Tracker des PANDA-Detektors durch Parallelisierung mit CUDA C*, Master Thesis, FH Aachen (2015)
- [10] Duda, R. O. and P. E. Hart, *Use of the Hough Transformation to Detect Lines and Curves in Pictures* Comm. ACM, Vol. 15, pp. 11-15 (January, 1972)
- [11] Böcher M, *Plane Analytic Geometry: With Introductory Chapters on the Differential Calculus* (H. Holt, 1915)